Sixth International Symposium on Turbulence and Shear Flow Phenomena
Seoul, Korea, 22-24 June 2009

# TURBULENT STRUCTURE OF BUBBLE FREE AND CONFINED JETS

**Yerbol K. Akhmetbekov[1,2], Sergey V. Alekseenko[1,2], Vladimir M. Dulin[1], Dmitriy M. Markovich[1,2,*], Konstantin S. Pervunin[1]**

1: Siberian Branch of Russian Academy of Sciences,
Institute of Thermophysics
Lavrentyev Avenue, 1, Novosibirsk, 630090, Russia
*: dmark@itp.nsc.ru

2: Department of Physics,
Novosibirsk State University,
Pirogova Street, 2, Novosibirsk, 630090, Russia

## ABSTRACT

The present work is devoted to the experimental study of bubble-saturated free and impinging turbulent jets (Re = 12,000) by using a planar fluorescence-based technique for bubble imaging, combined with PIV and PTV methods for the velocity measurements. The bubble jet flows were investigated under the various volume gas fractions. On the basis of 10,000 measured spatial distributions of the instantaneous velocity fields of the both phases and local gas fraction, the statistics on the turbulent fluctuations in the jets flows was calculated, including mixed one-point correlations. The paper reports the effects of volume gas fraction on turbulent fluctuations in liquid phase (suppression or enhancement) for free and impinging jet flows.

## INTRODUCTION

Interest in studies of two-phase bubbly flows is caused by that they often occur in nature and have many industrial applications, e.g. bubble columns are used extensively in chemical, biochemical and petrochemical reactors. In practice, liquids are often saturated with gas bubbles to intensify mass transfer between the phases via large interface area (even for relatively low void fractions) and due to bubble-induced wake vortices increasing the mixing rate. Two-phase mediums also prevail in absorption apparatuses, evaporators, scrubbers, air lifting pumps and other devices. The presence of dispersed phase in cavitation, aeration and flotation processes is known to have a crucial influence on the flow structure. Besides, the injection of small gas bubbles into wall-bounded flows can provide a decrease of the drag force.

Presently, the concept of coupled interaction of continuous and dispersed phases is widely acknowledged via a number of experimental, numerical and analytical works. Depending on bubble sizes and characteristic scales of turbulence, various effects take place. Trajectories of bubbles can be affected by anisotropic turbulent fluctuations in liquid phase (turbulent dispersion), while the motion of bubbles and their agglomerates has an impact on properties of turbulent fluctuations in the carrier phase (turbulence modulation) due to a number of physical mechanisms.

Because of their complexity, two-phase turbulent flows are often described and modelled by the use of averaging approaches (spatial and ensemble averaging). However, the averaged equations of motion remain unclosed, which necessitates the use of closure models. Thus, the development and verification of modern approaches (e.g., Reynolds-stress models) for simulation of sufficiently anisotropic turbulent multi-phase flows requires comprehensive experimental information to be retrieved. The mixed correlations of the liquid velocity and void fraction (including the third-order moments) are of a special interest in this case. With this, there is a need of the accurate data on simultaneously measured planar distributions of the instantaneous gas-phase and liquid-phase velocity and the gas fraction. However, the estimation of such data is a very challenging experimental task.

Starting from the works by Serizava et al. (1975) and subsequent ones (e.g., Lance and Bataille, 1991; Nakoryakov et al., 1996), a lot of experiments on the study of suppression or enhancement of turbulence by bubbles have been presented in literature. In most of them, however, pipe flows or bubble columns are considered, and the measurements are often restricted by distributions of the mean velocity and velocity pulsations of the phases, average fraction and particles sizes of the dispersed phase. In free-shear flows, such as jets, the mutual interactions between dispersed phase particles and large-scale eddies developing in the mixing-layer can significantly affect the turbulent structure of the whole flow. For example, on the basis of the wall shear stress measurements, Alekseenko et al. (1999) have shown the strong suppression of the large-scale vortices in the bubble jet impinging on a flat surface. Roig et al. (1998) studied the planar bubble mixing-layer by using an optical fibre probe and reported the distributions of the gas fraction, mean velocity of both phases, and r.m.s. velocity fluctuations. The authors demonstrated a self-similar evolution of the mean velocities of the phases and increase of turbulent fluctuations of continuous phase while adding the relatively small (with diameter close to the turbulence microscale) bubbles into the flow. It was also suggested that, for the studied two-phase flow, bubble velocity fluctuations were caused by both turbulent dispersion mechanism and self-induced fluctuating motions.

One of the latest works on the bubbly mixing layer study is the paper by Rightley and Lasheras (2000) where the interphase energy transfer in the planar free shear layer, saturated with bubbles, was investigated experimentally in detail. In order to study the role of large-scale vortices in the bubble dispersion and the energy redistribution within the carrier phase, the single-point measurements with a conditional sampling approach were carried out in the periodically forced mixing layer. Among the first articles, reporting the influence of the bubbles on the far field of turbulent free jets, the works by Sun and Faeth (1986a, b) can be mentioned, where the authors used LDA for the measurement of the gas and liquid flow velocity. For the estimation of sizes and spatial distribution of the bubbles, a flash photography technique, registering all the bubbles on the line-of-sight through the whole flow, was used. Besides, predictions of interphase momentum exchange effects were made on the basis of $k$-$\varepsilon$ calculations for the carrier phase and by using different assumptions for the two-phase turbulent flow. Near the jet axis the authors observed a slight increase of the turbulent kinetic energy of the liquid phase at $8d$ distance from the nozzle exit, when bubbles (about 1 mm in diameter that is near 5 times smaller than $d$) were added to the turbulent jet flow (Re ≈ 9,000). However, the effect of turbulent modulation was not very significant since the volume void fraction was small enough. Recently, Milenkovic et al. (2007a,b) studied the bubble trapping inside the large-scale vortices developing in the initial region of the periodically forced bubbly jet flow. The authors used a PIV system with conditional sampling approach to estimate the averaged velocity and vorticity of liquid phase. For the measurements of the void fraction and bubbles velocity, a double optical sensor was utilized. The high values of the bubbles concentration in centres of the large-scale vortices propagating along $r/d = 0.5$ were registered. However, in spite of a great interest from standpoint of CFD development, at the moment, practically no accurate experimental information on mutual statistics (i.e. one-point correlations) on velocities fluctuations of liquid and gas phase and gas fraction in turbulent bubbly jet flows can be found in literature. Thus, the aim of the present paper is the experimental study of the turbulent structure of the gas-saturated free and impinging turbulent jets by using planar optical measurement methods. The use of these techniques allowed to estimate simultaneously the spatial distributions of the instantaneous gas fraction and velocity of the both phases. The emphasis of the analysis was on the effect of the bubbles (with various volumetric gas fraction) on the structure of the turbulent jet flow.

## EXPERIMENTAL SETUP AND MEASUREMENT SYSTEM

The measurements were performed in a plexiglass working section (400 mm in height, 200 mm in width and 200 mm in length) which was the part of a hydrodynamic loop. The loop was equipped with a pump, which rotation speed was controlled by an inverter connected to a flowmeter. 10%-ethanol solution in distilled water was used as the working liquid. The liquid temperature was maintained constant at 30±0.2 °C by using a thermostat. The turbulent jet flows were organized by a contraction nozzle, located at the bottom of the working section, with the outlet diameter $d = 15$ mm. In case of the impinging jet flow, a flat plate was mounted normally to the jet axis at the distance $H = 3d$ from the nozzle edge. The Reynolds number, defined on the basis of the mean flow rate velocity $U_0 = 0.93$ m/s, kinematic viscosity of the working liquid $v$ and the nozzle diameter $d$ was equal to 12,000. The dispersed phase medium was an air that was supplied to a bubble generator by a compressor. The gas flow parameters were controlled by a thermometer, manometer and mass-flowmeter. The bubble generator of a special design provided a close-to-monodisperse distribution of the bubbles by size. The jet flows were investigated under the various volume gas fractions, $\beta$ (0%, 1.2%, 2.4% and 4.2%), while the mean bubble diameter was fixed, i.e., $D_b = 0.85$ mm. The volume gas fraction is given by

$$\beta = \frac{Q_g}{Q_g + Q_l} \qquad (1),$$

where $Q_g$ and $Q_l$ are the volume flow rates of the gas and liquid, respectively.

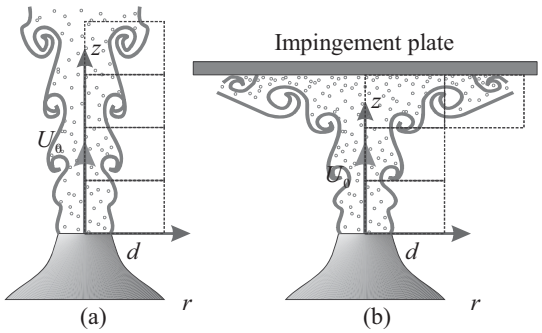


Figure 1. Schemes of disposition of elementary measurement zones for (a) free and (b) impinging jets.

A “PIV-IT” PIV-system consisting of a double-pulsed Nd:YAG laser (emission wavelength 532 nm, pulse duration 10 ns, energy per pulse 50 mJ), CCD camera (8 bits, 1240×1024 pixels) and a synchronization device was used for the measurements of the liquid phase instantaneous velocity. The system was operated by a computer with "ActualFlow" software. A laser sheet was formed by a system of focusing and cylindrical lenses; its width was approximately 0.5 mm in the measurement area. In order to avoid harmful glares (caused by reflection of the direct laser light) from the bubbles on the camera image, fluorescent tracers with the mean diameter of 20 μm and the range of emission wavelengths of 550-700 nm were added into the working liquid for carrying out the PIV measurements. A Micro Nikkor 60 lens equipped with a high-pass filter with steep transmission edge at 560 nm was mounted on the camera. Rhodamine B was utilized as the fluorescent dye for bubbles imaging via a planar fluorescence approach (see the next section); its concentration in the working liquid was about 90 μg/l.

The measurements were performed in the central plane of the jets, and in order to provide a high enough spatial resolution (final size of the interrogation area was 0.58 mm) the studied area was separated into four elementary zones where the measurements were performed independently

(see Figure 1a and b). For each zone and flow regime, 10,000 image pairs were captured by the camera to provide a sufficient number of events for statistics calculation of the dispersed phase velocity and concentration.

## IMAGES AND DATA PROCESSING

As was already mentioned, the bubbles located close to the central plane of the laser sheet were identified by applying a planar fluorescence-based technique. The technique is based on registration of the emission of a fluorescent dye dissolved in the working liquid when a laser light sheet illuminates it. The bubbles located near the central plane of the sheet (i.e. of the measurement plane) reflect and refract the diffusive emission of the dye and form bright rings on the camera image (see Figure 2). One of the major advantages of the technique is that an image of bubble located nearby the measurement plane (laser sheet plane) becomes defocused rapidly with increasing the distance between bubble and the plane. It allows to identify the bubbles locations and sizes only in a certain rectangular measurement area with a small thickness (about that of the laser sheet). Therefore, the bubble imaging method is rather local (even for a high depth of fields of a lens used) and can be successfully applied to bubble flows with volume gas fractions greater than the usual limit for shadow photography.

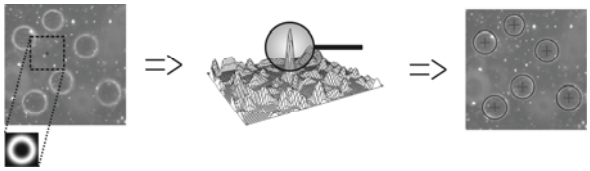

Figure 2. Scheme of correlation-based approach for bubble ring identification in PFBI images.

For the detection of the sharp rings (i.e. focused bubble images), a correlation-based procedure was elaborated. Bubbles' positions and sizes were determined by calculating a number of correlation fields between an original image and ring-like masks with different radii (see Figure 2). The highest peaks on the correlation planes corresponded to the best matching between the ring on the image and the mask with an appropriate radius. Approximation of the peak by a Gaussian function allowed the location of the bubbles to be determined with sub-pixel accuracy. When the bubbles were determined in each image of the pair, a matching procedure (i.e., a PTV algorithm) detected the same bubbles on the first and second images and allowed to evaluate the bubbles instantaneous velocity. The procedure utilizes a criterion of correlation similarity between the bubbles (including necessity for close values of radii) and allows to further increase the accuracy of the bubbles velocity estimation. When the bubbles are detected, a sharpness of the ring images is analysed and only focused bubbles are used in the further steps of processing. Besides, the problem of identification of highly overlapped bubble images was partially solved by using an adaptive scheme for the mask segmentation.

For estimation of the continuous phase instantaneous velocity, an adaptive iterative cross-correlation PIV algorithm with image deformation was used. The size of the final interrogation area was 32×32 pixels (0.576×0.576 mm), and the overlap rate of the areas was 50%). Obtained vector fields were validated and outliers (i.e., false vectors) were removed, including those caused by defocused bubbles in front of the laser sheet. Initially, the following signal-to-noise criterion was applied. Thereby, if the highest cross-correlation peak was not two times higher than the next one, the vector was considered to be false. Finally, an effective outlier removal procedure, namely, an adaptive 7×7 median filter (Westerweel and Scarano, 2005) was applied.

On the final stage, when the spatial distributions of the instantaneous velocity of both phases and bubbles locations and sizes were estimated basing on the each image pair analysis, the statistical moments were calculated using 10,000 samples for each zone and flow regime. During the statistics estimation, the spatial averaging of the bubbles data was performed with the same size of the averaging area (i.e., 0.58×0.58 mm) and overlap rate (i.e., 50%) as in PIV for the liquid phase. In grid points where neither bubbles were detected nor PIV velocity vector passed the validation routine, the gas phase fraction was considered to be unknown and such grid cells were not accounted in the statistics calculation. Otherwise, if the PIV vector passed the validation, the gas void fraction $\chi_b$ in such grid point was considered to be null or greater, depending on the fact if a bubble was detected here or not.

## RESULTS AND DISCUSSION

In this section, the spatial distributions of the mean velocity and gas fraction as well as the second-order moments of the velocity fluctuations are presented for the studied free and impinging bubbly jet flows. The effects of dispersed gas phase on the jet structure are described for the various volume gas fractions. The shown distributions correspond to raw experimental points, i.e., no data smoothing was done.

### Free Jet Flow

The examples of the spatial distributions of the local gas fraction, $\alpha = \langle \chi_b \rangle$, axial mean velocity of bubbles, $U_b$, and the mean square deviation, $\langle v_b^2 \rangle$, of the radial velocity fluctuations of the bubbles are shown in Figure 3 for the free jet flow at $\beta = 1.2\%$ with the average diameter of the bubbles $D_b = 0.85$ mm. One can observe that in the initial region of the flow, $\alpha$ is quite uniform in the jet core. However, locally large values ($\alpha \approx 0.02$) can be seen at $r/d \approx 0.5$ and $z/d \approx 0.2$. A similar local maximum was observed by Roig et al. (1998) in vicinity of the splitter plate of the bubbly mixing layer. In the present study, the maximum was also present for the other cases of $\beta$, and was considered to be caused both by a non-uniform bubble distribution inside the pipe preceding the contraction nozzle and by the effect of the wake zone after the nozzle rim. As in Roig et al. (1998), the downstream evolution of $\alpha$ demonstrates a fast decay of the peak and the distribution becomes more uniform. When the spatial distribution of the local gas fraction $\alpha$ was estimated, it can be used in (2) for the evaluation of the gas flow rate through a horizontal

cross-section of the jet. As the test case, the values (2) were estimated for the cross-sections $z/d = 0.2$ and 0.8 of the free jet flow at $\beta = 1.2\%$ and were found to be within 2% agreement with the value of $Q_g = 0.018$ l/s controlled by the mass-flow meter during the experiment.

$$Q_g = 2\pi \int_0^\infty \alpha U_b r dr \qquad (2)$$

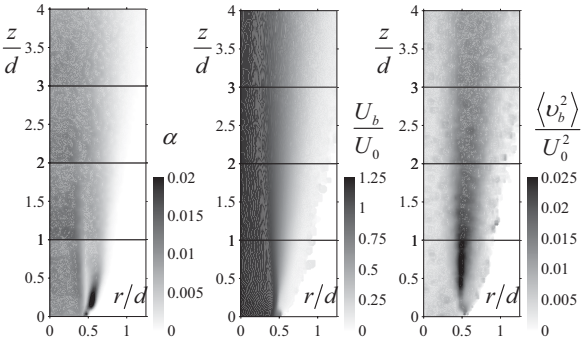


Figure 3. Spatial distributions of the (a) mean gas fraction, (b) axial mean velocity of bubbles and (c) second-order moment of the radial velocity fluctuations of the bubbles for a free jet flow with $\beta = 1.2\%$.

In general, for the studied cases of the bubbly free jets, the spatial distributions of the bubbles' mean axial velocity, $U_b$, were found to be rather similar to these of the liquid phase ($U_l$). The main difference observed was that $U_b$ was slightly greater than $U_l$ in the region of the jet core and in the mixing layer. For example, the comparison between axial mean velocities of the phases is shown in Figure 4 for two cross-sections. The first cross-section ($z/d = 0.5$) corresponds to the initial region of the jet, while the second one ($z/d = 3.5$) is at the edge of the measurement area. For the both cases, the profiles of $U_b$ and $U_l$ are quite similar, but due to the buoyancy force $U_b$ magnitude is slightly larger near the jet axis and in the outer mixing layer.

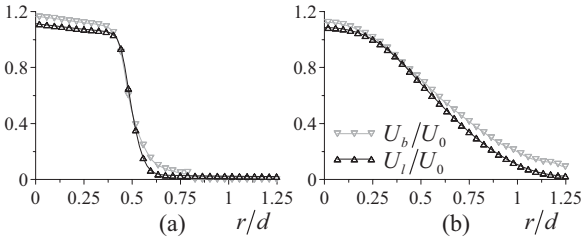


Figure 4. Profiles of the axial mean velocity of bubbles and liquid at (a) $z/d = 0.5$ and (b) $z/d = 3.5$ cross-sections of a free jet flow with $\beta = 1.2\%$. Each second experimental point is shown.

Note that for the both shown cross-sections (as well as for another ones), the difference in the axial mean velocities around $r/d = 0.5$ is almost absent. Thus, the generation of bubble-induced turbulence in this region is expected to be rather small. In general, in comparison to the single-phase flow, the influence of bubbles on the mean velocity of the liquid was found to be insignificant: increase of $\beta$ results in a growth of $U_l$ magnitude in the jet core while the shape of distribution undergoes practically no changes. In contrast, the influence of the bubbles on turbulent fluctuations is much more pronounced. The spatial distributions of the radial component of turbulent kinetic energy (TKE) of the liquid phase are presented in Figure 5 for the various values of $\beta$ (the mean bubble diameter was 0.85 mm). In the initial region of the jet (but after $z/d = 0.5$), values of $\langle \upsilon_l^2 \rangle$ are observed to decrease with $\beta$, while the location of a maximum is observed to shift upstream. In the vicinity of the nozzle rim ($z/d < 0.5$), the increase of $\beta$ resulted in a faster growth of $\langle \upsilon_l^2 \rangle$ (see also Figure 9a for more details). At the same time, no significant distinction was found at the edge of the tested area ($z/d \sim 4$).

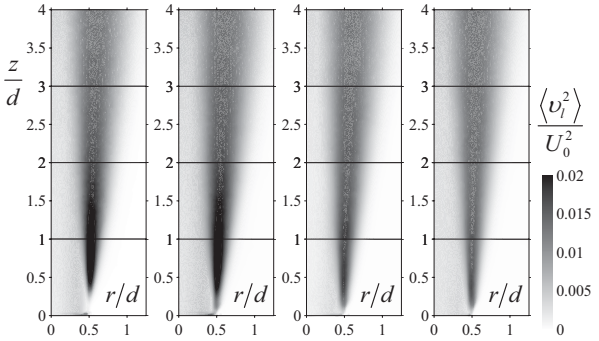


Figure 5. Spatial distributions of the radial component of TKE for free jet flows at (a) $\beta = 0\%$, (b) 1.2%, (c) 2.4%, and (d) 4.2%.

Figure 3c shows the spatial distribution of the second-order moment, $\langle v_b^2 \rangle$, of the bubble velocity fluctuations in the radial direction for the case $\beta = 1.2\%$. One can observe that $\langle v_b^2 \rangle$ is quite similar to $\langle v_l^2 \rangle$ (cf. Figure 3c and Figure5b), i.e., it has locally peak values in the jet mixing layer. Besides, in the initial region of the flow (near $r/d = 0.5$ and $z/d \approx 0.6$), $\langle v_b^2 \rangle$ also has the local maximum (about $0.027 U_0^2$) that is very close to the peak of $\langle v_l^2 \rangle$. Figure 6b, where the spatial distribution of the gas and liquid phase radial velocity fluctuations correlation $\langle v_l\, v_b \rangle$ is shown for the case $\beta = 1.2\%$, indicates the strong correlation between the velocity fluctuations. Besides, such strong correlation is also observed for the axial velocity (i.e., for $\langle u_l\, u_b \rangle$). Thus, it can be concluded that the bubble velocity pulsations (for the studied gas fractions) are mainly caused by turbulence in the liquid phase.

Figures 6c and d show the third-order moments, corresponding to the correlations between the axial and radial velocity fluctuations of the liquid with the gas fraction pulsations (note that $\chi_b' = -\chi_l'$), respectively. Actually, these quantities correspond to the difference between the conditionally-averaged and ensemble-averaged TKE components, i.e., $\langle \chi_l\, v_l^2 \rangle - \langle \chi_l \rangle \langle v_l^2 \rangle$ and $\langle \chi_l\, u_l^2 \rangle - \langle \chi_l \rangle \langle u_l^2 \rangle$. Generally, the difference is rather small in contrast to the absolute values of the TKE components (the liquid fraction $1-\alpha$ is about 0.99 in the jet core).

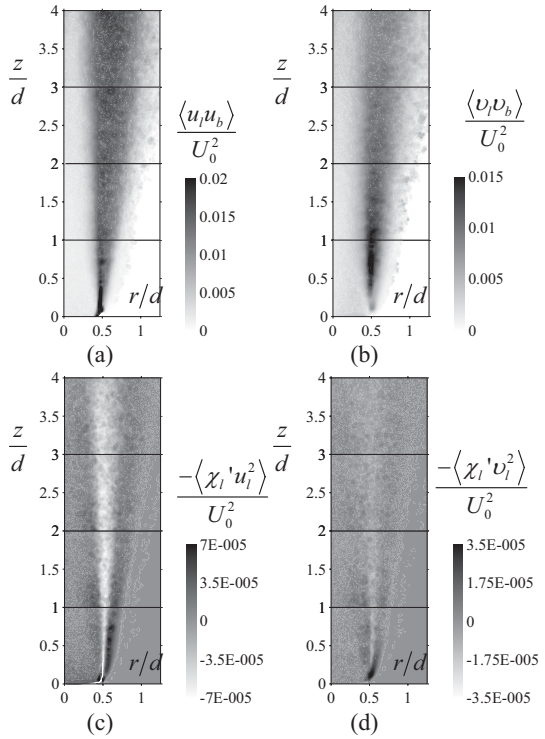


Figure 6. Spatial distributions of the (a, b) gas and liquid phase velocity correlations and (c, d) third-order moments of the liquid phase fraction and velocity fluctuations in a free jet at $\beta = 1.2\%$.

### Impinging Jet Flow

The present subsection presents the results of the experimental study of the impinging jet flow with the same initial distributions (gas fraction, bubble size, flow rate etc.) as for the free jet flow described above. The only difference is the impingement plate located at $3d$ from the nozzle exit.

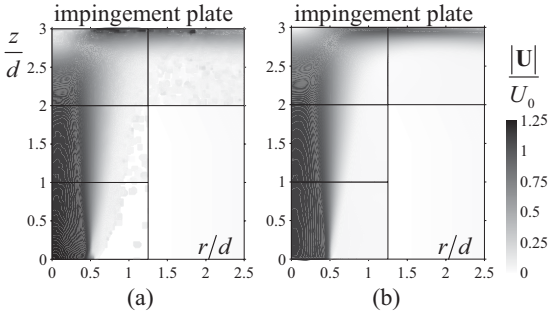


Figure 7. Spatial distributions of the mean absolute velocity of (a) bubbles and (b) liquid for an impinging jet. $\beta = 1.2\%$.

Figure 7 shows the spatial distributions of absolute mean velocity of both phases for the impinging jet flow with $\beta = 1.2\%$ and $D_b = 0.85$. In the initial region of the jet the distributions are quite similar to those of the free jet flow. However, in the region around the stagnation point ($z/d = 3$, $r/d = 0$) the difference in the mean velocity of the phases is more pronounced. First, a faster decay of $U_b$, in contrast to $U_l$, was observed for $z/d > 2.5$ due to increase of the mean pressure when approaching the impingement plate (see example in Figure 9b). At the same time, a radial pressure gradient tends to a faster growth of the radial bubble velocity in comparison to the liquid phase.

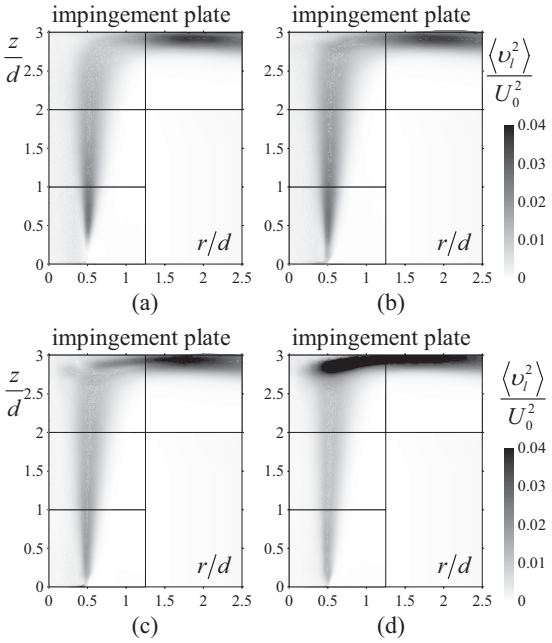


Figure 8. Spatial distributions of the radial component of TKE for impinging jet at (a) $\beta = 0\%$, (b) 1.2%, (c) 2.4%, and (d) 4.2%.

Spatial distributions of the radial TKE component for the liquid phase in the impinging jet flows with the different $\beta$ are shown in Figure 8. In the vicinity of the nozzle exit, one can observe that the bubbles effect on turbulence fluctuations in the liquid is similar to the free jet flow described above. Figure 9a, shows the profiles of $\langle \upsilon_l^2 \rangle$ along the shear-layer ($r/d = 0.5$) of the impinging bubbly jets with different $\beta$. For the free jet flow, the distributions were almost the same and, thus, are not shown. In all cases, an exponential growth of $\langle \upsilon_l^2 \rangle$ with $z$ is observed. The bubble presence resulted in a more rapid increase of $\langle \upsilon_l^2 \rangle$ near the nozzle edge ($z < 0.15d$). Both in the free and impinging jet cases the growth rate (i.e., value of $B$ if one approximates $\langle \upsilon_l^2 \rangle$ by a function $A \cdot \exp(B \times z/d)$) increases three times for the two-phase flow if one compares the cases of $\beta = 0$ and $\beta = 1.2\%$. For higher values of $\beta$ (2.4% and 4.2%) the effect is more pronounced. However, the difference in $U_l$ profiles, and consequently in the shear rate, for these cases was negligibly small. Moreover, as already mentioned, the $U_l - U_b$ in the shear layer ($r/d = 0.5$) was almost null for the whole tested area. Thus, the bubble-induced turbulence from the added mass effects is expected to be small and not responsible for the increase of the growth rate. The faster growth of $\langle \upsilon_l^2 \rangle$ was considered to be mainly caused by turbulent motions of the bubbles near the nozzle exit. An analysis of the initial distributions of fluctuations intensity of the liquid phase at the nozzle exit has shown an increase of the axial intensities in the jet core (from 4.4% to 6% of $U_0$). Near the impingement plate, as can be seen from Figure 8, the bubbles effect on turbulence in the liquid phase results in a significant increase of turbulent pulsations. For the two-phase jet with the smallest studied

gas content (i.e. $\beta = 1.2\%$), $\langle v_l^2 \rangle$ has a local maximum of $0.036U_0^2$ at $z/d = 2.9$, $r/d = 1.9$, while for $\beta = 4.2\%$ the maximum $0.09U_0^2$ appears at $r/d = 0.67$. Besides, the growth of $\langle v_l^2 \rangle$ values with $\beta$ takes place in the near-wall region. As discussed above, the significant difference in the mean velocity of the phases was observed in the high-pressure region near the impingement plate. For example, Figure 9b shows the difference in the velocities for the case $\beta = 1.2\%$ near the impingement plate along r/d = 0.5. Thus, it is concluded that for the impinging gas-liquid jet, the large values of $\langle v_l^2 \rangle$ along the wall were mainly caused by the bubble-induced turbulence in the high-pressure region and then were advected in the radial direction by the flow. Skewness factor, shown in Figure 10b for the case of $\beta = 4.2\%$ (the normalized third-order moment of $v_l$,) indicates the strong asymmetry (high negative values) of the liquid phase velocity fluctuations close to the impingement surface only for $r/d < 1.0$.

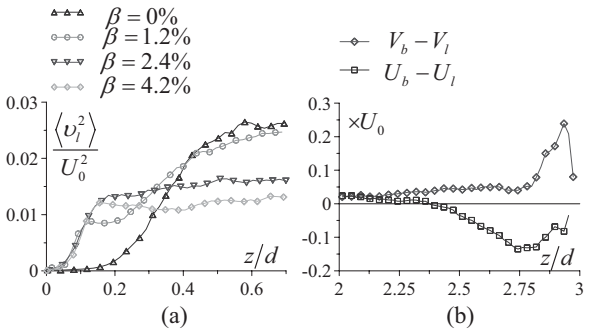


Figure 9. Profiles of the (a) radial component of TKE in liquid (various $\beta$) and (b) difference in the mean velocity of bubbles and liquid ($\beta = 1.2\%$) along $r/d = 0.5$ cross-section for the impinging bubbly jet flows. Each second experimental point is shown.

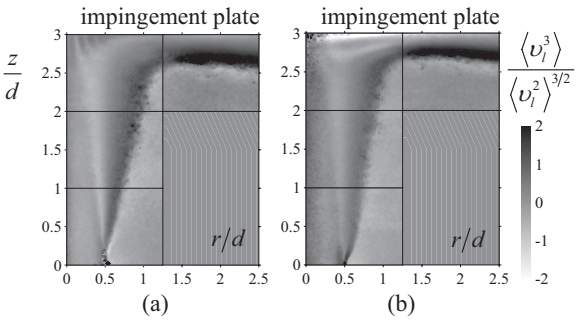


Figure 10. Spatial distributions of the skewness factor of the radial velocity fluctuations of liquid in an impinging jet at (a) $\beta = 0\%$ and (b) 4.2%.

## CONCLUSIONS

The paper reports the results of the experimental study of the bubbles effect on the turbulent structure of the gas-saturated free and impinging jets at Re = 12,000 and volume gas fractions up to 4.2%. Spatial distributions of the instantaneous liquid and gas velocities and local gas fraction were measured by planar optical techniques and a set of statistical moments, including the third-order mixed correlations, was estimated. It was concluded that the dispersed phase influences mainly the turbulent structure of the flows while the mean velocity distributions, in comparison to the single-phase flows, are almost unchanged in the studied range of gas fraction. It is shown that in the initial region of the jet shear layer, the injection of bubbles leads to a faster growth of the liquid-phase velocity fluctuations. Downstream ($z/d > 0.3$), the bubble presence resulted in suppression of the liquid-phase velocity fluctuations and such a difference was clearly observed until $z/d < 3.5$. For the impinging jet flow, similar observations were made for the region near the nozzle exit and for the jet mixing layer. In the near-wall region, along the impingement surface, it was found that the liquid velocity fluctuations dramatically increase with volume gas fraction due to bubble-induced turbulence in the high-pressure region around the stagnation point, where the bubbles produce strong asymmetry of the liquid velocity fluctuations.

## ACKNOWLEDGEMENTS

The work is supported by integration research projects of RAS and SB RAS and by RFBR (grant N 07-08-00213).

## REFERENCES

Alekseenko, S. V., Markovich, D. M., and Semenov V. I., 1999, "Suppression of large-scale structures in a gas-saturated impact jet", *Technical Phys. Lett.*, Vol. 25, pp. 374-376.

Lance, M., and Bataille, J., 1991, "Turbulence in the liquid phase of a uniform bubbly air-water flow", *J. Fluid Mech.*, Vol. 222, pp. 95-118.

Milenkovic, R. Z., Sigg, B., and Yadigaroglu, G., 2007a, "Bubble clustering and trapping in large vortices. Part 1: Triggered bubbly jets investigated by phase-averaging", *Int. J. Multiphase Flow*, Vol. 33, pp. 1088-1110.

Milenkovic, R. Z., Sigg, B., and Yadigaroglu, G., 2007b, "Bubble clustering and trapping in large vortices. Part 2: Time-dependent trapping conditions", *Int. J. Multiphase Flow*, Vol. 33, pp. 1111-1125.

Nakoryakov, V. E., Kashinsky, O. N., Randin, V. V., and Timkin, L. S., 1996, "Gas-liquid bubbly flow in vertical pipes (Data Bank contribution)", *J. Fluids Eng.*, Vol. 118, pp. 377-382.

Rightley, P. M., and Lasheras, J. C., 2000, "Bubble dispersion and interphase coupling in a free shear flow", *J. Fluid Mech.*, Vol. 412, pp. 21-59.

Roig, V., Suzanne, C., Masbernat, I., 1998, "Experimental investigation of a turbulent bubbly mixing layer", *Int. J. Multiphase Flow*, Vol. 24, pp. 35-54.

Serizava, A., Kataoka, I., and Michigoshi, I., 1975, "Turbulence structure of air-water bubbly flow – II. Local properties", *International Journal of Multiphase Flow*, Vol. 2, pp. 235-246.

Sun, T. Y., and Faeth, G. M., 1986a, "Structure of turbulent bubbly jets – I. Methods and centerline properties", *Int. J. Multiphase Flow*, Vol. 12, pp. 99-114.

Sun, T. Y., and Faeth, G. M., 1986b, "Structure of turbulent bubbly jets – II. Phase property profiles", *Int. J. Multiphase Flow*, Vol. 12, pp. 115-126.

Westerweel, J., and Scarano, F., 2005, "Universal outlier detection for PIV data", *Exp. Fluids*, Vol. 39, pp. 1096-1100.